The Journal of Experimental Biology 204, 1855–1867 (2001)
Printed in Great Britain © The Company of Biologists Limited 2001
JEB3368

THE VORTEX WAKE OF THE FREE-SWIMMING LARVA AND PUPA OF *CULEX PIPIENS* (DIPTERA)

JOHN BRACKENBURY*

Department of Anatomy, Downing Street, Cambridge CB2 3DY, UK

*e-mail: jhb1000@mole.bio.cam.ac.uk

Accepted 8 March 2001

Summary

The kinematics and hydrodynamics of free-swimming pupal and larval (final-instar) culicids were investigated using videography and a simple wake-visualisation technique (dyes). In both cases, swimming is based on a technique of high-amplitude, side-to-side (larva) or up-and-down (pupa) bending of the body. The pupa possesses a pair of plate-like abdominal paddles; the larval abdominal paddle consists of a fan of closely spaced bristles which, at the Reynolds numbers involved, behaves like a continuous surface. Wake visualisation showed that each half-stroke of the swimming cycle produces a discrete ring vortex that is convected away from the body.

Consecutive vortices are produced first to one side then to the other of the mean swimming path, the convection axis being inclined at approximately 25° away from dead aft. Pupal and larval culicids therefore resemble fish in using the momentum injected into the water to generate thrust. Preliminary calculations for the pupa suggest that each vortex contains sufficient momentum to account for that added to the body with each half-stroke. The possibility is discussed that the side-to-side flexural technique may allow an interaction between body and tail flows in the production of vorticity.

Key words: *Culex pipiens*, larva, pupa, swimming, kinematics, hydrodynamics, vortex wake.

Introduction

Our present understanding of the ways in which the bodies of swimming and flying animals interact with the fluid environments in which they live to generate propulsive force has been greatly increased by flow visualization studies. Fish (McCutchen, 1977; Blickhan et al., 1992; Videler, 1993; Muller et al., 1997; Drucker and Lauder, 1999; Wolfgang et al., 1999), tadpoles (Liu et al., 1997), bats (Rayner et al., 1986), birds (Spedding et al., 1984; Spedding, 1986; Spedding, 1987) and insects (Van den Berg and Ellington, 1997; Grodnitsky, 1999) transfer momentum into the wake in the form of parcels of vorticity that are often visibly ring-like in shape. Similar studies have not yet been carried out on swimming invertebrates, but circumstantial evidence from the Reynolds numbers involved and the structure of the swimming organs suggests that even quite small (<1 cm in length) aquatic arthropods can exploit the inertial properties of the water to enhance propulsive force generation. Nachtigall (Nachtigall, 1961; Nachtigall, 1962; Nachtigall, 1963) argued that the faster and more efficient swimming of certain aquatic dipterans such as larval and pupal culicids, in comparison with related forms such as ceratopogonid and chironomid larvae, was related to the possession of abdominal paddles.

Larval and pupal culicids both use large-amplitude, unilateral bending movements of the body for swimming, rather than the sinusoidal movements characteristic of many other aquatic invertebrates such as ceratopogonid fly larvae (Nachtigall, 1961), nematode worms (Gray and Lissman, 1964), leeches (Kristan et al., 1982) and mayfly larvae (J. Brackenbury, personal observations). Unilateral bending brings the extremities of the body into contact or near contact at the end of each stroke, lending at least the theoretical possibility of a beneficial hydrodynamic interaction between the extremities, body and tail flows combining to augment vortex production. Such interactions are known to occur in fish during continuous, straight-line swimming (Muller et al., 1997; Wolfgang et al., 1999) and during turning (Wolfgang et al., 1999). During continuous undulatory swimming, the body generates a flow that later interacts with and modifies the flow downstream of the tail. During C-starting, which is more comparable kinematically with culicid swimming, the body and tail generate flows simultaneously, allowing interaction as the flow is generated. An additional feature to be considered in the case of the culicid larva and pupa is the structure of the paddle: whereas that of the pupa is a conventional, fin-like plate, the larval paddle is in the form of a fan of bristles. The larval body also possesses additional tufts of bristles that have not hitherto been considered in a locomotory context but which could have a hydrodynamic function. Thus, the immature stages of *Culex pipiens* show similarities in kinematic performance but also areas of contrast in design and possibly performance. The present study examines the hydrodynamic performance of these insects using a simple wake-visualisation technique.

Materials and methods

Final-stage larval instars (body length 1.0±0.1 cm, *N*=10; body mass 9.4 mg, *N*=10) and pupae (body length 0.75 cm, *N*=10; body mass 9.7 mg, *N*=10; means ± S.D.) of *Culex pipiens* (L.) were collected from local pools and ditches in the Willingham Fen district, northwest of Cambridge, UK. The insects were transferred to indoor tanks where they were maintained at ambient temperatures of 18–22 °C, similar to the outdoor temperatures prevailing at that time of year (spring and early summer). Organic debris from the parent pools was retained with the water samples to provide a suitable micro-environment for the micro-organisms on which the larvae continued to feed. Swimming behaviour was filmed using a NAC 400 high-speed video system (NAC Inc., Japan) with slave-driven stroboscopic illumination, delivering 200 or 400 frames s^{-1} and additionally, in daylight conditions, with a Panasonic video camera (S-VHS format, horizontal resolution >400 lines) delivering 50 fields s^{-1} (horizontal resolution >200 lines) at a shutter speed of 0.001 s. Video tapes were viewed on a cassette recorder with a single-field advance facility, allowing detailed examination of kinematic and hydrodynamic events. Swimming trajectories and water flow in the vicinity of the insects were traced by hand directly from the video screen.

Larvae and pupae both habitually rest at the water surface attached to the surface tension film by their respiratory siphons. Swimming can be elicited by tapping the container or a nearby surface, and the pupa typically dives downwards at a steep angle to a depth of several centimetres then commences a series of bobbing movements or 'mini-dives' each consisting of a few strokes of downward motion followed by flotation. Alternatively, a mini-dive may be extended into continuous swimming. The larva usually escapes from the surface at a shallower angle than the pupa, and its motion tends to be in the horizontal plane rather than downwards.

The method of flow visualization made use of a harmless red food-colouring agent (E122) suspended in water and glycerol (specific gravity of suspension 1.012 g $m1^{-1}$) which was dispensed into the medium either in drops from a hand-held syringe or as a narrow (approximately 1–2 mm) streamer from a plungerless syringe body mounted above the water, with its needle tip just penetrating below the surface, and discharging the dye slowly under the force of gravity. In both cases, the speed of descent of the dye through the water was only a fraction of the speed of the swimming insects and the water currents produced during swimming. At the start of an experiment, one or two insects were removed from the holding tank and transferred to a transparent container measuring 8 cm (height) × 6 cm (width) × 3 cm (depth). The field of view of the camera was set to cover the frontal area of the container. The relatively small size of the test chamber served to maximise the likelihood of interception between the swimming insect and the added dye. Additional observations were made using the streamer technique on insects swimming in a larger container measuring 16 cm (height) × 8 cm (width) × 8 cm (depth) although, because of the larger volume of water involved, the frequency of 'hits' was lower. To enhance image contrast, the insects were viewed against a white card placed behind the container.

The drop and streamer techniques produced reliable data for individual swimming strokes but, because of their 'hit-or-miss' nature, they were less effective in detailing the chain of events associated with a succession of strokes. Consequently, in the second method, a 2–3 cm layer of dye was carefully laid down

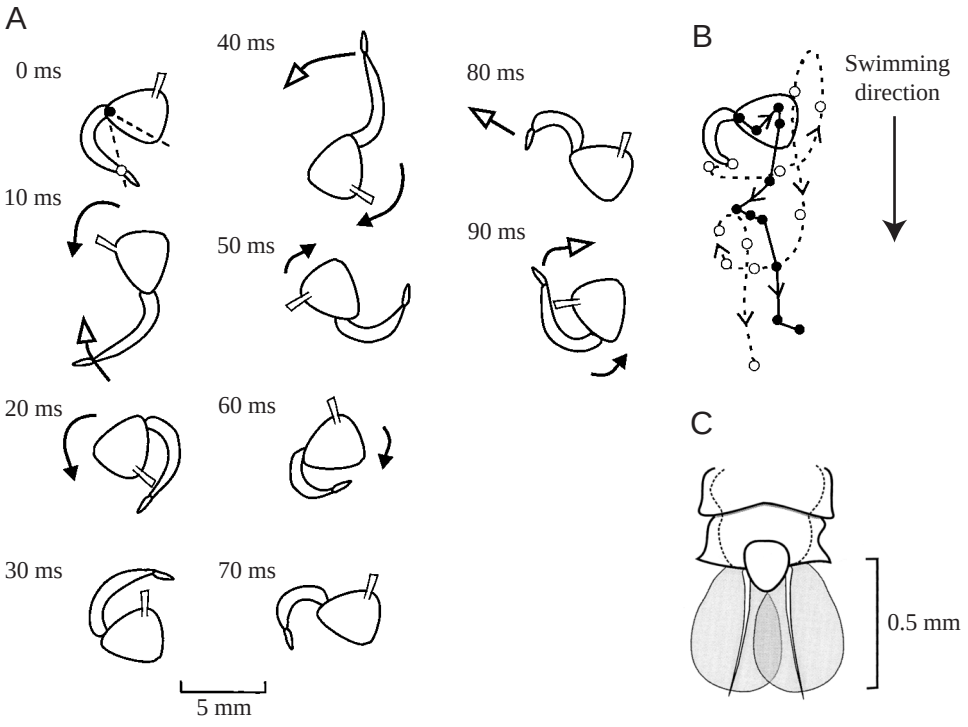

Fig. 1. Kinematic events at the start of a pupal mini-dive. (A) Body profiles at 10 ms intervals from the start of diving (0 ms). The dorsal surface of the insect is indicated, in this and the following figures, by the projecting respiratory siphon. The filled and open circles in the resting position indicate the centre of gravity of the body and the abdominal paddles, respectively. The dashed lines indicate the position of the radius vector from the base to the tip of the abdomen in the resting and full-down (end-downstroke) positions. Arrows with open or filled heads indicate the direction of rotation of the abdomen and head/thorax about the centre of gravity, respectively. (B) The motion of the centre of gravity and abdominal paddles at the stages corresponding to those shown in A. (C) Abdominal tip and paddles.

on the bottom of the container through a syringe needle, making sure that a sharp interface between the slightly denser dye layer below and the clear water above was preserved. In these circumstances, the initial dive from the surface usually took the pupae into the dye layer, from which they then emerged by flotation and, beginning their bobbing behaviour, broke up the interface, causing the wake to be visualized. Approximately 250 insects of each stage were investigated, the bulk of the quantitative data being based on approximately 150–200 swimming bouts in each case. Results are presented as mean values ±1 S.D. unless stated otherwise.

Results

Pupal kinematics and hydrodynamics

A mini-dive may be brief, lasting for only one or two strokes of the abdomen followed by flotation back towards the surface, or it may be extended into sessions of continuous downward swimming interrupted by brief periods of passive flotation towards the surface. In these latter cases, the total period of immersion (dive duration) may last up to nearly 1 min. In a random sample of 20 dives, dive duration was 6–58 s with a mean of 22 s. The kinematic events associated with the start of a mini-dive are illustrated in Fig. 1. Immediately before the dive, the pupa floats with the longitudinal axis of the head/thorax capsule aligned with the horizontal and the abdomen curled beneath the body in its characteristic resting posture (0 ms position in Fig. 1A). In this position, taking a radius from the base of the abdomen, where it pivots with the thorax, to its tip, the abdomen lies 38.6±5.7 ° (*N*=15) short of the full end-downstroke position achieved during normal swimming. In the latter case, the tail plates are almost in contact with the head/thorax (Brackenbury, 1999). It follows that a dive invariably begins with an upstroke, but this is an abnormally short upstroke, the abdominal tip sweeping through approximately 290 ° with respect to the head rather than the usual 330 ° (Brackenbury, 1999). The counter-rotation of the body around the centre of gravity, here assumed to lie at the pivot between the thorax and the abdomen, is correspondingly reduced from its normal value of 398.5 ° to 355.4±24 ° (*N*=16). This initial upstroke drives the centre of gravity directly forwards, i.e. horizontally, and it is the ensuing downstroke that sets the body on its downward course and establishes the normal oscillatory rhythm of the body that alternately rotates nose-down then nose-up, through 399 °, with consecutive half-strokes (Fig. 2C). The path pursued by the centre of gravity during continuous swimming tacks above (upstroke) and below (downstroke) the mean swimming path through 26 °, whilst the leading edge of the head/thorax capsule and the abdominal tip perform cycloidal movements either side of the mean swimming path (Fig. 2A,B). Between half-strokes, there is a brief pause during which the abdomen is motionless and the abdominal paddles are held against or in near contact with the dorsal (end-upstroke, positions 1, 11 and 12 in Fig. 3A) or ventral (end-downstroke, positions 4 and 5 in Fig. 3A) surface of the head/thorax capsule.

Although the body appears to the naked eye to advance smoothly along its path, the centre of gravity accelerates to a maximum velocity near the middle of each half-stroke then decelerates momentarily to zero at the beginning of the pause in abdominal activity (Fig. 3A,B). Note that, during this pause, the body continues to rotate around the centre of gravity (Fig. 3C,D). Maximum forward velocity of the body coincides with the peak in the angular motion of the abdomen around its pivot with the thorax (Fig. 3C). This occurs in the middle of the side-to-side swing of the abdomen, which is also the point at which the abdominal paddles reverse their motion with respect to the water. Thus, most of the acceleration of the body takes place during the phase of backward motion of the paddles, but forward movement continues after the paddle has itself begun to move forward during the passive rotatory period.

The dye traces show that each half-stroke results in the production of a discrete ring vortex that is shed at an acute angle

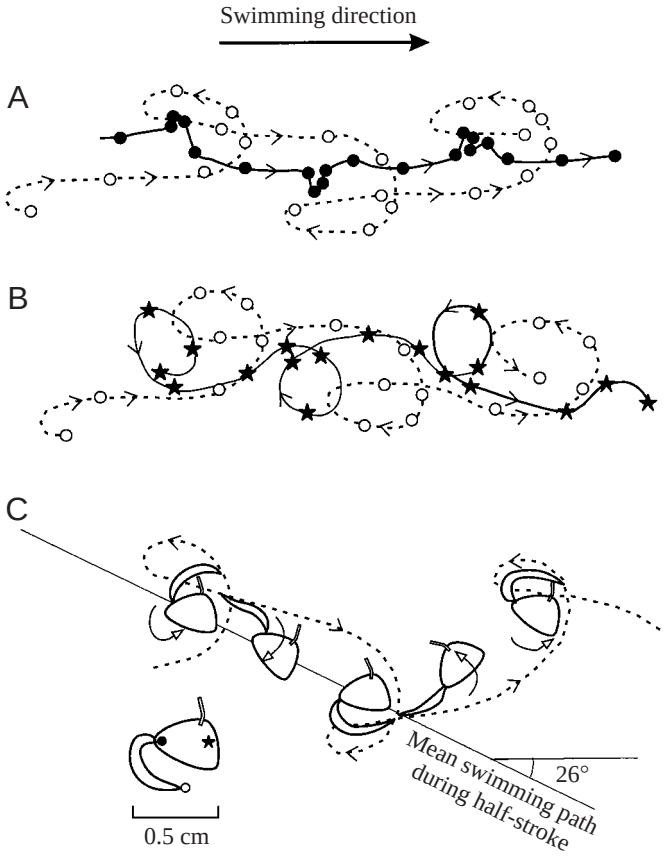

Fig. 2. (A,B) Kinematic events during a complete cycle of continuous swimming in the pupa. The traces show motion of the centre of gravity (filled circles), the abdominal paddles (open circles) and the leading edge of the head/thorax capsule (stars). (C) Cartoon sequence of the stroke starting on the left with the abdomen curled above the head/thorax at the end of the preceding upstroke. Note how the mean path of the body tacks downwards through 26 ° during the downstroke and upwards through 26 ° during the upstroke relative to the mean forward swimming path. A, B and C are from different swimming events.

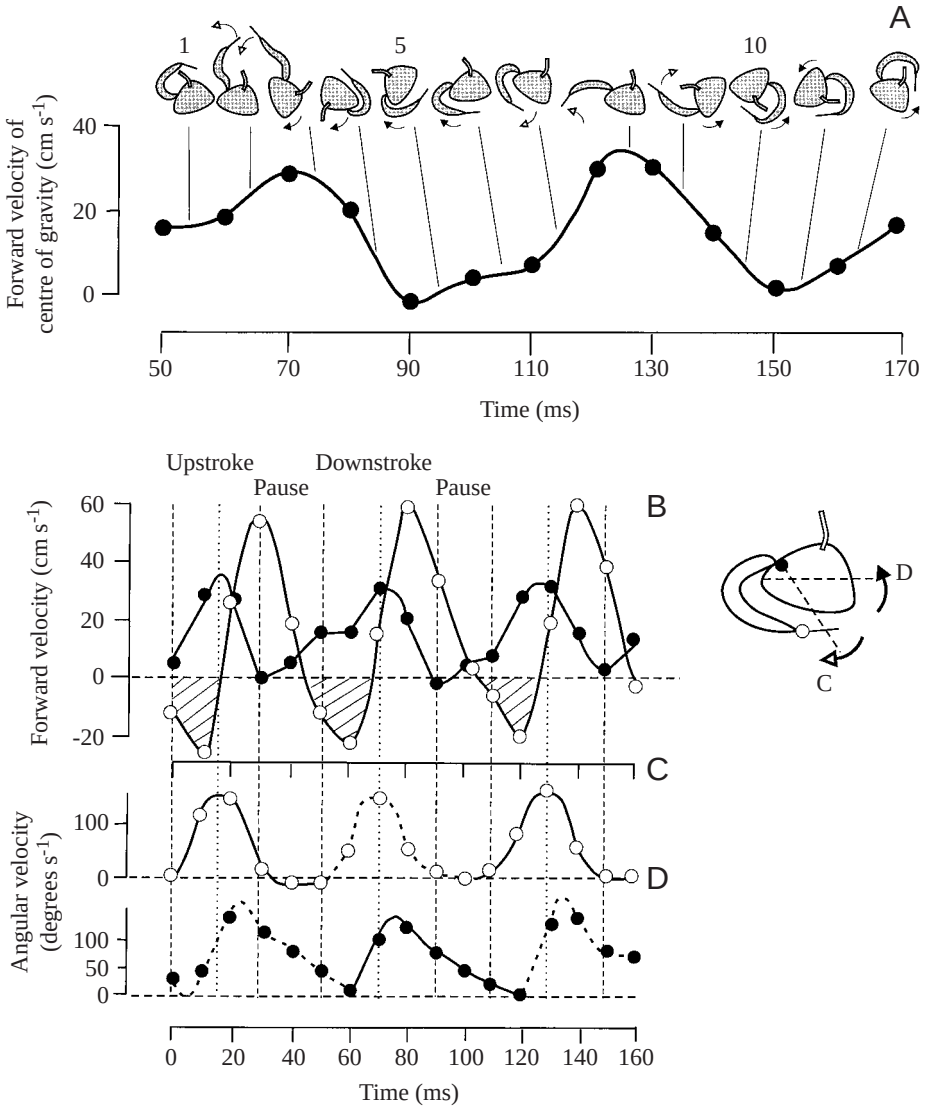

Fig. 3. Kinematic variables during continuous swimming in the pupa. (A) Changes in the forward velocity of the centre of gravity relative to the water during a complete downstroke/upstroke cycle. The cartoons represent the configuration of the body at the corresponding points in the cycle. Open and filled arrowheads represent the motion of the abdomen and head/thorax, respectively, around the centre of gravity. (B) Changes in the forward velocity component of the centre of gravity (filled circles, also shown in A) and the abdominal paddles (open circles). The hatched parts of the graph represent the parts of the swimming cycle when the abdominal paddles are moving backwards with respect to the mean swimming path through the water. (C) Changes in the angular velocity of the abdominal paddles about the centre of gravity, relative to the longitudinal axis of the head/thorax: this motion is indicated by the open-headed arrow in the cartoon on the right. (D) Changes in the angular velocity of the longitudinal axis of the head/thorax about the centre of gravity, relative to the water. This motion is indicated by the filled arrow in the cartoon on the right. The vertical dotted lines in B–D indicate the point, in the middle of a half-stroke, when the forward velocity of the centre of gravity is at its peak. The dashed lines demarcate the half-strokes and pause periods.

to the rear of the path of the body. The vortices were most clearly shown at the start of a mini-dive as the floating pupa emerged through the dye/water interface then dived back into it (Fig. 4). The shape of the vortex only became defined gradually as it moved away from the body because of the manner in which it was infiltrated by the dye. The first sign of the vortex was a movement of dye into its trailing edge, from which dye accelerated along the axis and progressively invaded the ring (see Fig. 6). This invasion was complete within 100–140 ms. The progress of the dye front was most clearly discernible once it had reached the centre of the ring, and this is the point at which the first measurements of the position of the dye front in Figs 5 and 6A were made. The distance between the first two data points for each vortex divided by the time interval (20 ms) therefore represents the maximum velocity of the induced jet at the ring plane and, as the data points show, the velocity of the dye front falls off thereafter as the dye reaches the leading edge of the vortex and recirculates into the ring. The last two recorded dye-front position data points for each vortex in Figs 5 and 6 therefore represent the motion of the leading edge of the vortex as it moves away from the body.

The convection velocity of the vortex is the velocity at which the vortex moves away from the body, relative to the surrounding water. The jet velocity, here defined as the velocity at the centre of the ring, is therefore the sum of the convection velocity and the velocity due to the internal circulation within the ring. This interpretation is consistent with the results of experiments in which individual vortices passed directly through a vertical streamer of dye (Fig. 7). In 17 such cases, the ratio of the jet velocity at the ring plane to the convection velocity of the vortex was 2.10±0.15. As expected, the axial velocity of the dye steadily diminished towards the leading edge (Fig. 6B). Although the centre of the core of the ring could be located, the core radius could not be measured reliably. The external radius R_e and ring radius R (the distance between the centres of the opposite cores; Fig. 6) were 0.30±0.10 cm (N=21) and 0.21±0.10 cm (N=21) respectively.

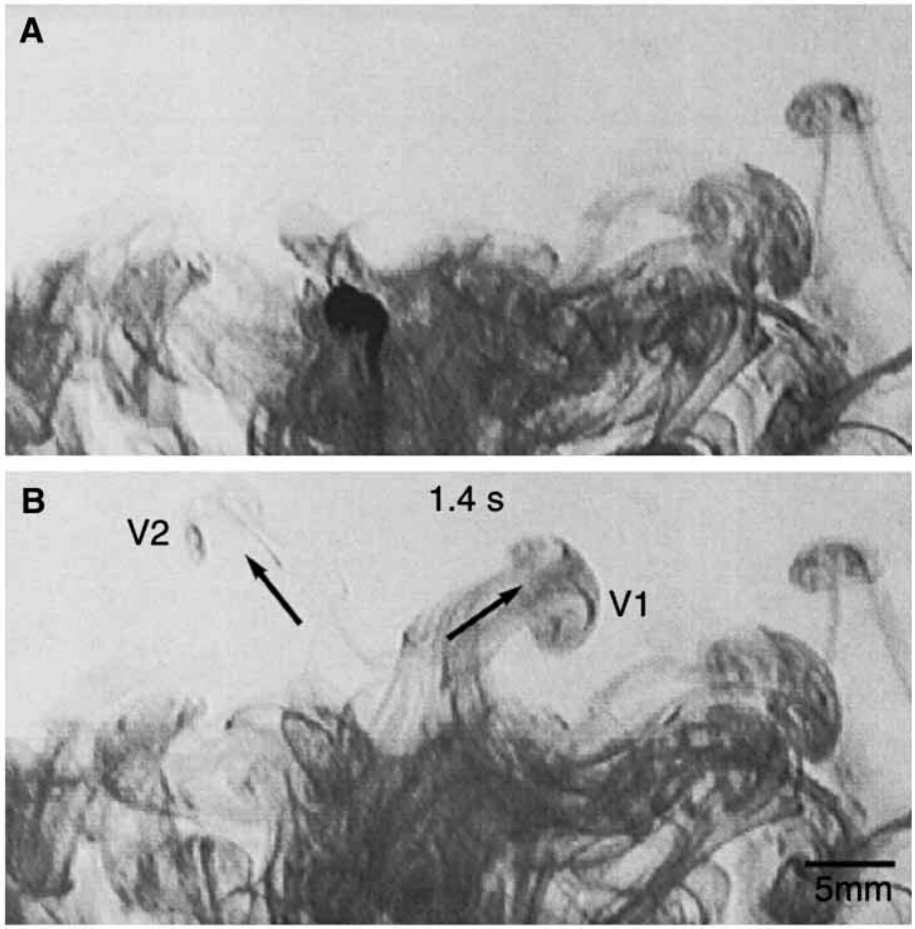

Fig. 4. Vortex production during a mini-dive by the pupa. (A) The pupa is floating towards the surface following its initial dive into a layer of dyed water on the bottom of the container. To the right can be seen a number of vortices associated with previous dives. (B) 1.4 s later, the pupa has dived out of sight, leaving behind two ring vortices produced by the first upstroke (V1) and first downstroke (V2). The arrows show the convection axes of the vortices.

Fig. 5 and Fig. 6A detail the motion of the dye front along the convection axis of the first three vortices associated with the first three half-strokes of the mini-dive. These figures also show the motion of the centre of gravity of the pupa; it can be seen that the vortices are shed behind and to the side of the swimming path. The convection axes of the vortices were directed above, i.e. dorsal, to the mean swimming path during the downstroke and below, i.e. ventral, to the main swimming path during the upstroke. The angle subtended between the axes of the first two vortices was 75° (Fig. 6) although, once continuous swimming was under way (see below), the vortices moved slightly closer to the midline, consecutive vortices being shed ±26° of dead aft of the swimming path.

The velocity of the dye front at the level of the ring plane, i.e. that measured between the first and second data points for each vortex in Fig. 6A, was 12.5 cm s^{-1}. By the definition given above, this is the jet velocity. The data in Fig. 6 are from 62 individual dives, the positions of the dye front and the centre of gravity being expressed with respect to the resting pupa (the 0 ms position indicated). The estimated convection velocity, for the jet velocity to convection velocity ratio of 2.1 given above, was therefore 6.0 cm s^{-1}. The mean velocity of the centre of gravity over the first three half-strokes, measured by summing the total path length between the first and last data points in Fig. 6A, was 13.5 cm s^{-1}. This is only slightly less than the mean forward velocity measured during continuous swimming (Table 1), suggesting that the pupa attains a mean steady-state speed within a few half-strokes of the start of diving.

The precise moment in the swimming cycle when the vortex was shed from the body of the pupa could not be established with certainty. As explained above, the vortex had been in existence for at least 20–40 ms before the first flow data were recorded. The data shown in Fig. 5 show considerable variation but suggest that, taking into account the delay in registering the presence of the vortex, it is shed during the second half of the abdominal stroke and before the passive

Table 1. *Kinematic and hydrodynamic data for* Culex pipiens *larvae and pupae during steady swimming*

	Pupae	Larvae
Swimming speed (cm s^{-1})	15.0	10.9±2.0 (19)
Swimming speed (*BL* s^{-1})	20.0	10.9
Stroke rate (s^{-1})	10.05	9.6±1.9 (19)
Distance travelled per stroke (*BL* $stroke^{-1}$)	2.0	1.13
Counter-rotation of body per half-stroke (degrees)	399	132±9 (51)
Tacking angle of body (degrees)	±26	±24±1.5 (51)
Reynolds number	1125	1090
Angle of vortex propagation axis (degrees from dead aft)	26.3±12.1 (66)	23.5±14.7 (41)
Body length (cm)	0.75	1.0±0.06 (10)
Body mass (mg)	9.7	9.4

All pupal data except the angle of vortex propagation axis are from Brackenbury (1999).

Body mass was determined as the mean of 10 animals weighed together.

BL, body length.

Values are means ± S.D. (*N*).

rotational phase has intervened. Note that it is also within this period that the forward velocity of the body peaks then drops towards zero (Fig. 3A).

The above description of wake formation is based on the first 300 ms or so of the start of swimming, but continuous straight-line swimming presented a much less clear picture since the swimming path rarely coincided with a sufficiently long stretch of dye interface, or length of streamer, to accommodate a sequence of half-strokes. In some cases, a jet of dye was seen moving along the axis of a presumed vortex shed at an angle of 26° above or below dead aft (Fig. 8). These jets, however, were only visible for approximately 50–100 ms and did not evolve into spherical vortices. Failure to do so may have been real, but is just as likely to have been due to methodological limitations. The clear exception was those occasions when vortex shedding coincided with a tight turn (Fig. 8, Fig. 9). In these cases, the half-stroke on the outer bend of the turn produced a persistent and fully formed vortex similar to those seen at the start of swimming. As Fig. 8 shows, a 'stopping vortex' was also observed during tight turns, travelling forwards and crossing the path of the turning vortex.

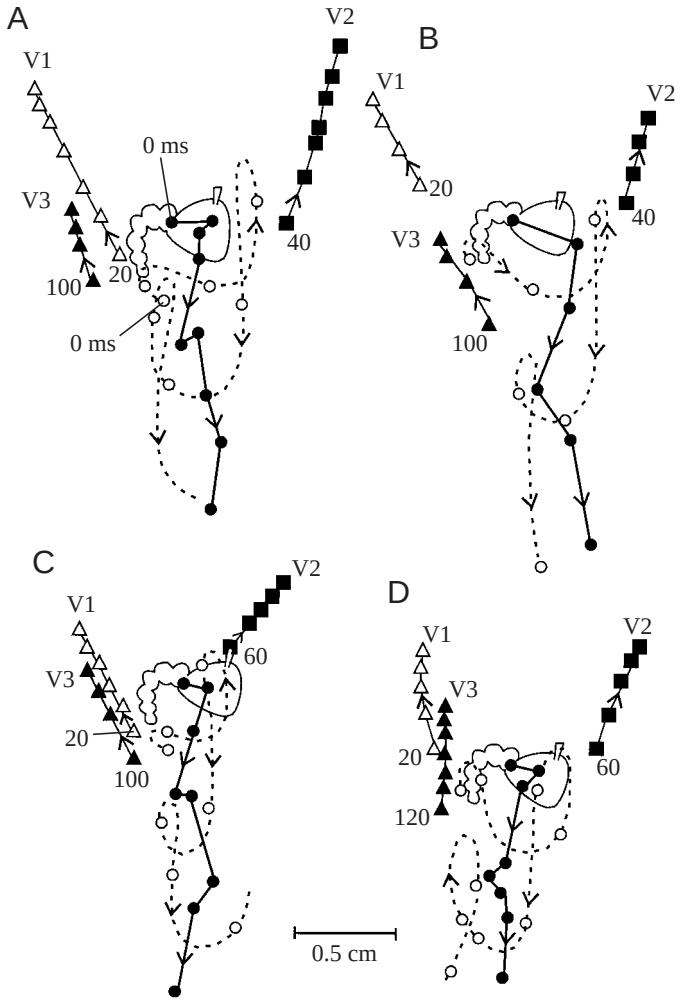

Fig. 5. Simultaneous kinematic and hydrodynamic events during the first three half-strokes of a pupal mini-dive. Data points plot the motion of the centre of gravity (filled circles), the abdominal paddles (open circles) and the dye front moving along with the associated vortices (V1–V3) (open triangles, filled squares and filled triangles, respectively) at 20 ms intervals. The data are from four individual dives, and the cartoon shows the starting orientation in each case (0 ms position). Arrows show the directions of movement of the dye front along the propagation axis of the vortex and of the centre of gravity and abdominal paddles.

Larval kinematics and hydrodynamics

The kinematics of larval swimming is illustrated in Fig. 10 and Fig. 11. Propulsion results from side-to-side flexure of the body, the abdominal tip sweeping through nearly 360° relative to the head during each half-stroke. Over the same period, the head/thorax counter-rotates through 132°. The path pursued by the centre of the thorax tacks to the left then the right of the mean swimming path through 24° (Fig. 10) and, as in the case of the pupa, the abdominal tip traces out a cycloidal path either side of the mid-line (Fig. 11A,B). Since the head faces backwards during swimming, the impression is given that the insect is drawn backwards by the lashing movements of its abdomen. As in the pupa, the forward velocity of the centre of the thorax surges to a maximum just after the middle of the stroke as the anterior and posterior halves of the body flex rapidly towards one another (profiles 3, 4 and 8, 9 in Fig. 10). Most of the acceleration of the centre of gravity, assumed to lie at the junction between the thorax and the abdomen, coincides with the period when the abdominal tip is being driven backwards relative to the mean swimming direction (hatched areas in Fig. 11C), although the peak velocity of the centre of gravity occurs slightly after this point.

A discrete ring vortex is produced during the rapid flexural stage of each half-stroke. The data shown in Fig. 12 are based on the first vortex produced at the start of swimming. The axis of the vortex lies at right angles to that of the initially extended body and intersects it half-way along its length. The axial velocity of the jet associated with the vortex, calculated from the distance travelled by the dye front during the first 20 ms of its motion, was 7.1±1.5 cm s^{-1} (N=42), or 57% of the axial velocity of the jet associated with the pupal vortex. The velocity of the centre of gravity of the larval body in the opposite direction during the first 20 ms of its motion was 11.2±2.4 cm s^{-1} (N=38). The external radius of the vortex R_e and the ring radius R were 0.42±0.05 cm (N=20) and 0.30±0.05 cm (N=20) respectively.

Structural features

The abdominal paddles of the pupa consist of a pair of plates approximately 0.5 mm in length (Fig. 1C). The larval abdominal tip is forked, with a dorsal respiratory siphon and a ventral fan of bristles. The latter are 5 μm in width and are arranged in 14 groups each comprising 10–12 bristles attached to a common base (Fig. 13A). The spacing between the bristles varies from the tip to the base of the fan, but at

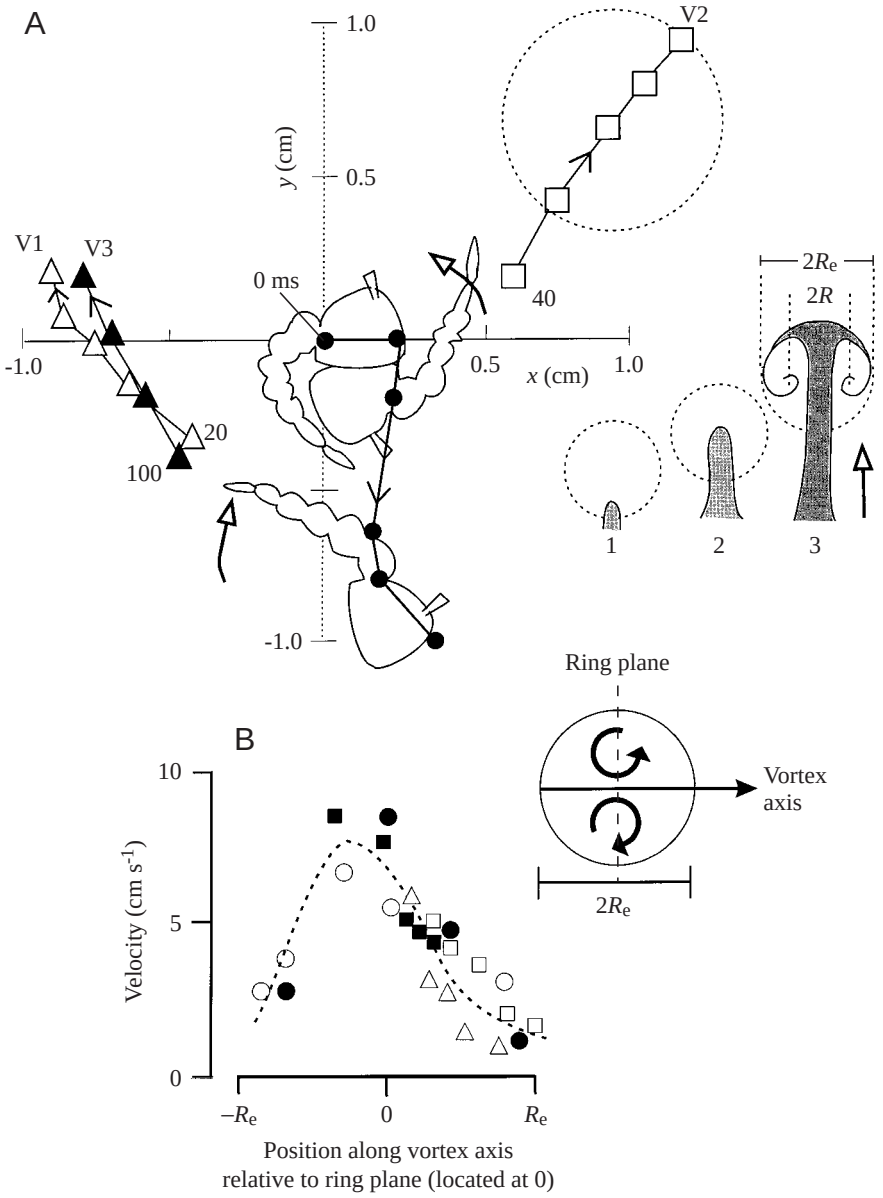

Fig. 6. (A) Pooled data from 62 individual pupal dives. For each data point, the *x*,*y* coordinates were plotted relative to the starting (0 ms) position of the centre of gravity. Points were measured at 20 ms intervals and show the motion of the centre of gravity (filled circles) and the dye front associated with the vortices (V1–V3; open triangles, open squares and filled triangles, respectively). The three profiles represent (from top to bottom) the configuration of the body in the resting position (0 ms) and in the middle of the second and third half-strokes (40 ms and 80 ms positions of the centre of gravity). The S.E.M. for each data point was similar to or smaller than the symbol width, so error bars are not shown. Open-headed arrows show the angular motion of the abdomen about the centre of gravity; arrows on the vortices indicate the motion of the dye front along the axis of the vortex. The dashed circle indicates the size and position of the spherical vortex at the time of the final data point. The cartoon, on the right, is a scheme of the movement of the dye front into the vortex. Initially, the dye is drawn into the trailing edge of the vortex (cartoon 1); it then moves along the axis to the centre of the ring (cartoon 2). At a later stage (cartoon 3), the dye has recirculated into the ring: the leading edge of the dye front is now coincident with the leading edge of the vortex and travels with the same velocity as the vortex. R and R_e are the ring radius and external radius of the vortex, respectively. (B) The velocity of the dye front along the centre line of five individual ring vortices. It was difficult to obtain data over the trailing half of the vortex axis. The dashed line is drawn by hand. The cartoon on the right of B represents a median section through a vortex travelling in the direction of the straight arrow.

mid-length it is approximately 7 μm. Two prominent tufts of bristles are also borne on each side of the thorax, each consisting of 13 units 5 μm in diameter (Fig. 13B). These bristles are feather-like, carrying two series of finer units or microtrichia that emerge at 5–7 μm intervals along the length of the bristle. Each michrotrichium is approximately 75 μm in length; consequently, although the spacing between the bristles half-way along the length of the tuft is of the order of 40 μm, the microtrichia divide the space into a matrix of cells of approximately 5 μm in width. The thoracic tufts bend in response to the hydrodynamic forces experienced during the second half of the stroke as the anterior and posterior portions of the body move together in the pincer movement associated with vortex production. Fig. 13C shows how the tufts on the inner side of the U-shape created by the flexing body become bent forwards towards the head.

Discussion

Operating at whole-body Reynolds numbers in the region of 10^3 (Table 1) makes it probable that both the final-stage larva and the pupa of *Culex pipiens* generate most of their propulsive force from inertial rather than viscous forces (Wu, 1977). Flow-visualization studies have shown that fish (McCutchen, 1977; Blickhan et al., 1992; Muller et al., 1997; Drucker and Lauder, 1999; Wolfgang et al., 1999), tadpoles (Liu et al., 1997), birds (Spedding et al., 1984; Spedding, 1986; Spedding, 1987), bats (Rayner et al., 1986) and flying insects (for a review, see Grodnitsky, 1999) transfer momentum into the fluid environment in the form of regulated bursts of vorticity. The three-dimensional structure of the wakes varies according to the different animals studied. In fish, for example, a three-dimensional chain of linked ring vortices has been postulated on theoretical grounds (Lighthill, 1969; Lighthill, 1970; Videler, 1993) and

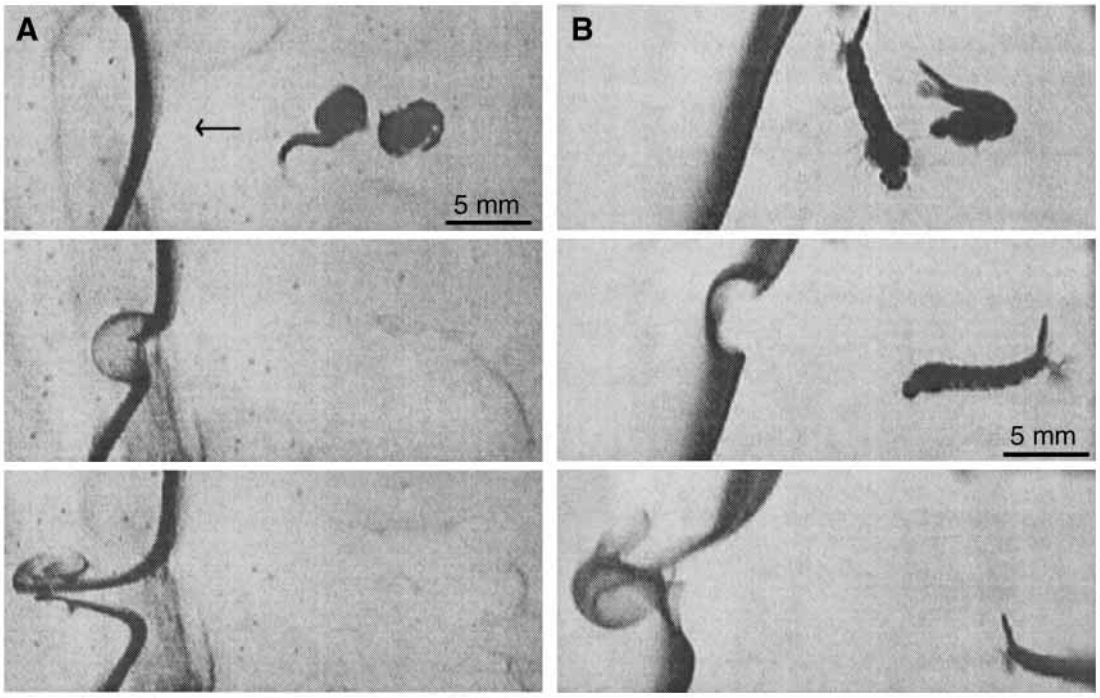

Fig. 7. Vortex production in (A) a pupa and (B) a final-stage larva. In A, the top videograph shows two consecutive stages, at 20 ms intervals, in the execution of a downstroke. The two images have been superimposed on the same frame and separated horizontally for clarity. A vortex has been produced by the end of the stroke and is travelling towards the dye streamer on the left in the direction of the arrow. After 80 ms, the leading edge of the vortex hits the streamer, and after a further 140 ms (middle videograph) it emerges from the other side of the dye streamer with its outline faintly showing through the dye, a plug of dye being drawn into the centre of the vortex. After a further 100 ms (bottom videograph), the dye that entered the vortex is now recirculating back into the ring. In B, the top videograph shows two superimposed and horizontally separated images of the larva viewed from above flexing to its right side. 20 ms later, the leading edge of the vortex produced by the body contraction has reached the streamer, and after a further 100 ms has almost passed through the streamer (middle videograph). The outline of the leading edge of the vortex is faintly visible, and a plug of dye is being drawn into the centre of the vortex. 200 ms later (bottom videograph), the dye that entered the vortex is now recirculating back into the ring.

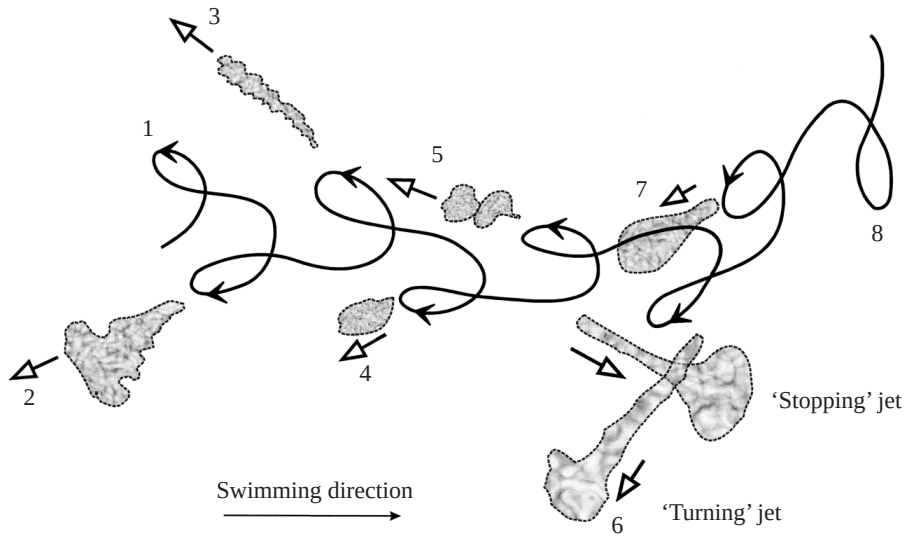

Fig. 8. Vortex production during continuous swimming in the pupa. The solid line traces the path of the tip of the abdominal paddle. Numbers 1–8 indicate half-strokes, and the jets of water associated with them are shown as stippled regions outlined by dashed lines. The open-headed arrows show the direction of the jets, which are orientated at ±26° from dead aft of the swimming path. The jets were traced directly from a video sequence. Each jet appeared in the second half of the stroke as the abdominal tip began to move forward relative to the water. The jets were usually only visible for approximately 50 ms, but in this case between the fifth and sixth half-strokes the insect turns upwards; this was accompanied by the release of a persistent jet on the outside of the bend. This jet, labelled number 6 in the drawing, is crossed by a forwardly directed 'stopping jet' associated with the change in direction.

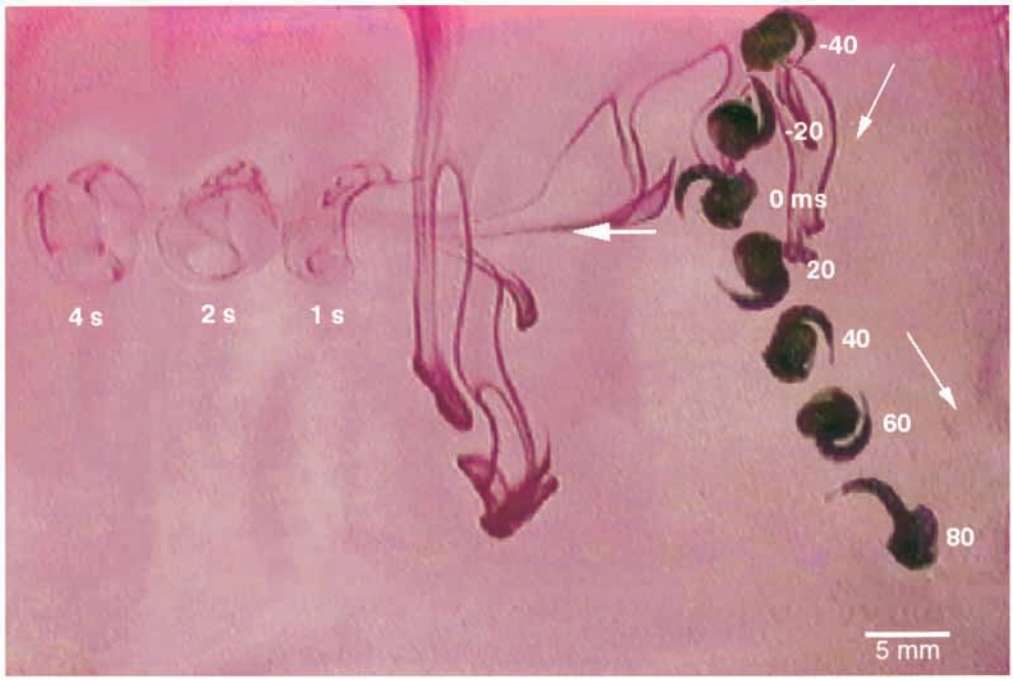

Fig. 9. Composite videograph of vortex generation by a pupa during the performance of a turn. The vortex is produced by a downstroke that begins at the 0 ms position and is complete by the 40 ms position of the pupa. Its production is associated with a change in swimming direction of approximately 60° (the angle between the two smaller arrows). The vortex travels to the left in the direction of the large white arrow. The dye pattern corresponds to the position of the vortex 1 s after its production, by which time it has travelled approximately 3 cm from the 0 ms position of the pupa. During the same period, the pupa disappeared from the lower right of the screen. Superimposed on the videograph are the images of the vortex 2 s and 4 s after its formation. Note that the vortex corresponds to the turning vortex shown in Fig. 8; the stopping vortex also illustrated in that figure is not visible here because of the absence of dye in the relevant area. The dye pattern in the middle of the videograph is a streamer falling slowly from the surface of the water.

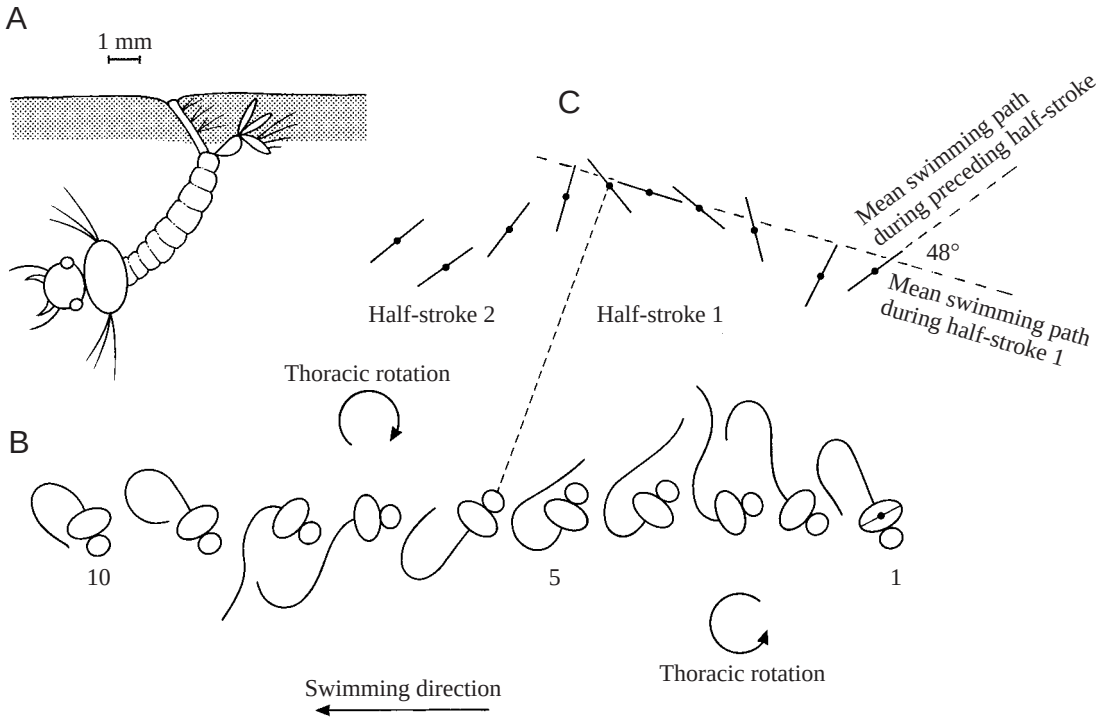

Fig. 10. Kinematics of continuous swimming in the final-stage larva of *Culex pipiens*. (A) Schematic illustration of the larva resting at the surface of the water. Note the respiratory siphon and tracheal gills and associated hairs. (B) Cartoon sequence illustrating a single cycle of swimming movements. The cartoons represent body profiles seen from the dorsal side at 10 ms intervals. The horizontal scale has been expanded to allow separation of the profiles. The dot on the animal in position 1 is the centre of the thorax, and the line intersecting it is the transverse axis of the thorax, changes in the orientation of which are illustrated in C. (C) The path of the centre of the thorax (dot) and the transverse axis of the thorax (line) through the water. Note how the axis of the thorax rotates through 132° throughout the half-stroke (compare profiles 1 and 5 in B) and the centre of the thorax tacks from side to side through 48°. The dashed line between B and C links corresponding stages (stage 6).

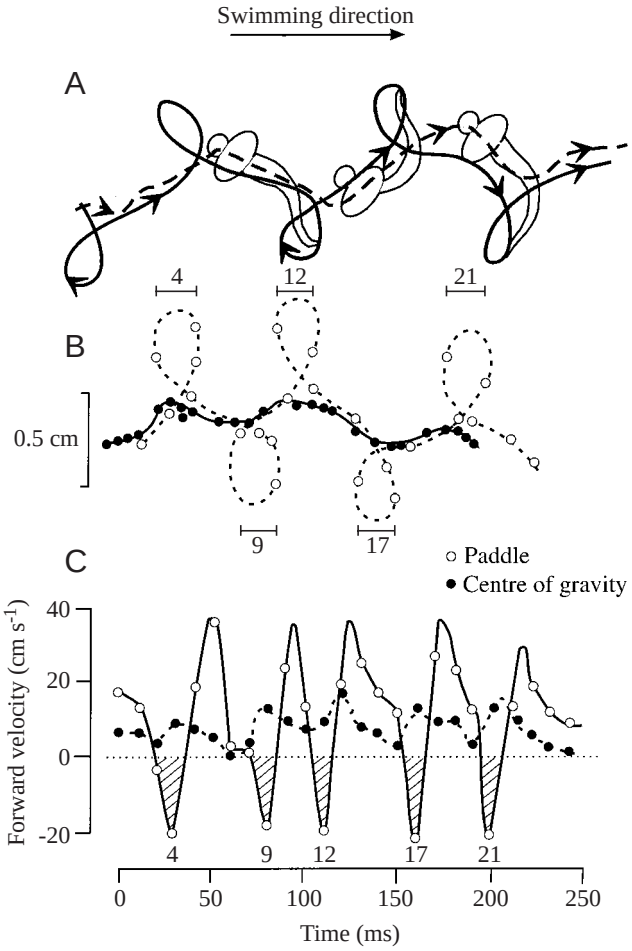

Fig. 11. Kinematics of continuous swimming in a final-stage larva. (A) Semi-schematic depiction of the path followed by the centre of gravity (dashed line) and the abdominal tip (continuous line) during two swimming cycles. The centre of gravity is assumed to lie at the junction between the thorax and the abdomen. The superimposed profiles represent the configuration of the body just after the half-way points in the cycle when the body is beginning to flex rapidly and the abdominal tip travels backwards with respect to the mean swimming path through the water. (B) The path of the centre of gravity (filled circles) and the abdominal tip (open circles) at 10 ms intervals. (C) The forward velocity of the centre of gravity (filled circles) and the abdominal tip (open circles). The hatched areas in C represent the period when the abdominal tip is travelling backwards through the water relative to the mean forward swimming direction. The numerals in C are the velocities calculated from the corresponding intervals between points shown in B.

confirmed by particle velocimetry (Muller et al., 1997; Wolfgang et al., 1999). Use of the pectoral fins produces trains of discrete, unlinked ring vortices (McCutchen, 1977, Fig. 15, p. 355; Drucker and Lauder, 1999). In the case of flying birds, Spedding et al. (Spedding et al., 1984) postulated that the bursts of vorticity should be composed of closed vortex loops, probably in the form of small-cored vortex rings. This model was largely vindicated by studies of slow-flying birds, although there was a deficit between the momentum measured within the rings and that needed to support the weight of the bird in the air. Spedding (Spedding, 1987) concluded that the wake may contain undetected complex structures that account for the missing impulse.

The present study furnishes qualitative evidence that, like the animals listed above, swimming pupal and larval culicids also inject momentum into the water in the form of vortices. These vortices are ring-like and are produced discretely, one for each half-stroke. Furthermore, the vortices are convected away from the body and the wakes of these insects therefore differ from those of the swimming fish studied by Muller et al. (Muller et al., 1997) and Wolfgang et al. (Wolfgang et al., 1999), which consist of standing vortices, linked into a chain, with a zig-zag caudal jet flowing through the centres of the vortices. The single vortex ring wake of culicids is similar to the wake of intermittent swimmers such as zebra fish *Brachydanio rerio* (McCutchen, 1977) and pectoral-fin swimmers at low speed (Drucker and Lauder, 1999). The flow-field data of the present study are insufficient to allow accurate measurement of the momentum and energy content of the vortices but, since it is important to know whether an approximate momentum balance exists between the moving insect and the vorticity that it generates, a crude estimate of these quantities in the pupa is presented here. Assuming, for the moment, that the vortex meets the appropriate geometrical criteria, i.e. that it is a small-cored ring vortex with a core radius to ring radius ratio of 0.25 or less, the momentum M of such a ring can be expressed as:

$$M = \rho\pi R^2\Gamma\,, \tag{1}$$

(Spedding et al., 1994), where ρ is the density of the medium, R is the ring radius and Γ is the circulation.

In fact, culicid vortices appear to be larger-cored, with a core radius to ring radius ratio of approximately 0.3, so the conditions for the application of equation 1 may not be met. The circulation in this equation can be obtained by integrating the fluid velocity component normal to the plane of the ring down the centre line of the vortex. The data contained in Fig. 6A allow an estimate to be made of the central velocity of the jet at the ring plane V_{jet}. In addition, the velocity profiles of the vortices shown in Fig. 6B suggest that a crude estimate of the circulation ($m^2\,s^{-1}$) can be made using:

$$\Gamma = V_{\text{jet}}R_{\text{e}}\,. \tag{2}$$

The momentum of the vortex ($kg\,m\,s^{-1}$) can therefore be expressed as:

$$M = \rho\pi R^2 R_{\text{e}} V_{\text{jet}}\,. \tag{3}$$

Inserting values of 0.002 m, 0.003 m and 0.125 $m\,s^{-1}$, respectively, for R, R_{e} and V_{jet} in equation 3 and taking ρ=1000 $kg\,m^{-3}$ yields a value for the momentum of 0.52×10^{-5} $kg\,m\,s^{-1}$. During each half-stroke, the centre of gravity of the pupal body is accelerated from rest to approximately 0.3 $m\,s^{-1}$ (Fig. 3A); consequently, with a body mass of approximately 10 mg, its peak momentum is 0.3×10^{-5} $kg\,m\,s^{-1}$. This very rough calculation therefore

suggests that there is sufficient momentum within the vortex to account for the momentum imparted to the body during each half-stroke. The low value for body momentum may be due to an error in the location of the centre of gravity, and it does not take account of the rotational momentum.

Although the swimming techniques of the pupa and final-stage larva may appear superficially quite different, they generate hydrodynamic force using the same fundamental body movement: a high-amplitude, unilateral flexure that brings the extremities of the body into contact, or near-contact, at the end of each half-stroke. The larval vortex is generated during the second half of the stroke (Fig. 7B, Fig. 12) as the anterior and posterior halves of the body come together in a pincer-like movement. The flow data, together with the morphological evidence from the bending of the thoracic bristles (Fig. 13C), are not incompatible with a scheme in which the two ends of the body generate vortices of opposite sign that eventually fuse to form a ring vortex. Thus, for example, the rapid body flexure to the left produces a vortex in reaction to which the body is accelerated to the right. The dynamics of this process differ from those involved in turning in fish, as reported by Wolfgang et al. (Wolfgang et al., 1999). In this case, rapid curvature of the backbone into a C-shape leads to fluid being drawn into, not forced out of, the C-shaped cavity as two oppositely signed vortices develop around the head and tail ends of the body. Subsequent straightening then leads to the body-generated vortices being shed into the wake as a thrust jet that drives the fish in the direction of flexure. This comparison shows that apparently similar kinematic events may have different hydrodynamic repercussions in different animals. Nevertheless, culicids and C-flexing fish are comparable in that the body and tail produce flow simultaneously; hence, the interaction between the flows takes place while they are being generated. This distinguishes them from undulatory swimmers in which the body generates a flow that later interacts with and modifies the flow downstream of the tail.

Nachtigall (Nachtigall, 1962; Nachtigall, 1963), in noting the faster and more efficient swimming of culicid larvae and pupae compared with chironomid and ceratopogonid larvae, attributed their superior performance to the possession of abdominal paddles. The present study confirms this in that it shows that culicid larvae and pupae derive propulsive force by accelerating water into their wakes. Although the paddle may not be the only part of the body involved in the generation of vorticity, as discussed above, it appears to perform just as effectively in the larva as in the pupa even though the larval paddle is a fan of bristles whilst the pupal fan is a more conventional continuous plate (Fig. 1C, Fig. 13A). The circumstances in which a bristled appendage would be expected to perform either as a rake for combing through the water or as a continuous surface for paddling the water were investigated by Cheer and Koehl (Cheer and Koehl, 1987). Their model is based on the assumption that each unit in a spatial array of bristles imposes a local shear gradient on the flow through the array which therefore influences its ‘leakiness’, i.e. the ratio of through-flow to the volume swept out by the appendage. The leakiness index of a particular array is governed by its geometry, namely the diameter and spacing of the bristles, and the Reynolds number of the bristles, based on their velocity relative to the far field. In general, as Reynolds

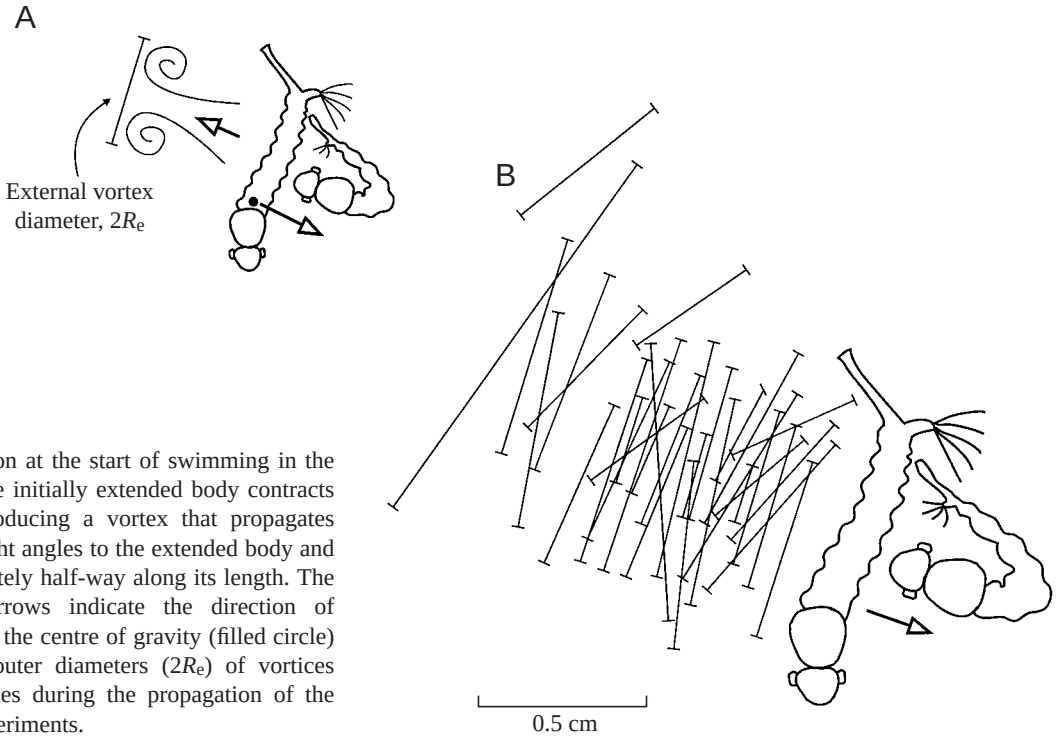

Fig. 12. Vortex production at the start of swimming in the final-stage larva. (A) The initially extended body contracts rapidly to one side, producing a vortex that propagates along an axis lying at right angles to the extended body and intersecting it approximately half-way along its length. The straight open-headed arrows indicate the direction of motion of the vortex and the centre of gravity (filled circle) of the body. (B) The outer diameters ($2R_e$) of vortices measured at various times during the propagation of the vortex in 33 separate experiments.

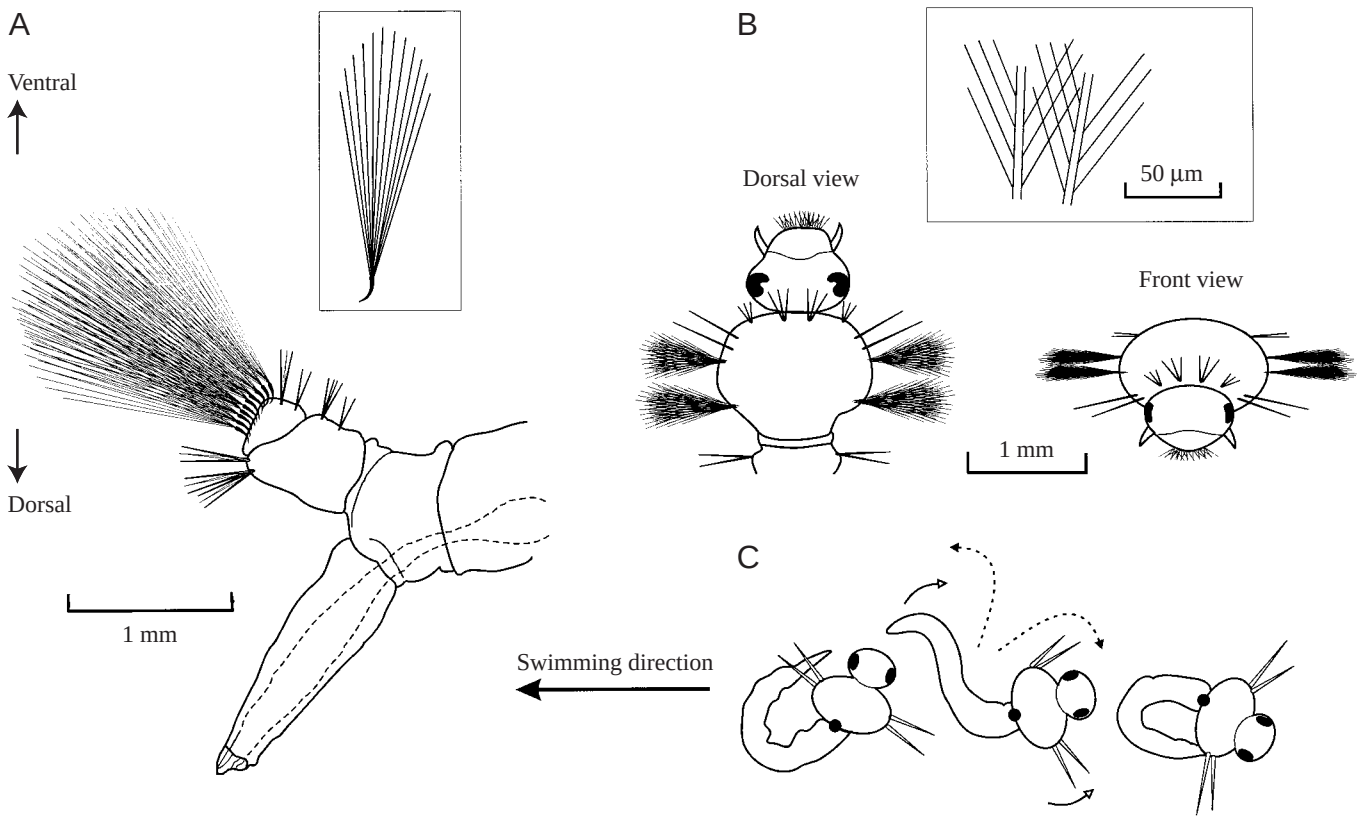

Fig. 13. Structure of the abdominal paddle and thoracic bristle tufts of the final-stage larva. (A) Abdominal tip showing details of the fan-like paddle. The inset shows an individual tuft of 12 bristles from the fan. (B) Details of thoracic bristle tufts. Each of the four tufts consists of 13 bristles: the inset shows two bristles at higher magnification. (C) Drawings from a video sequence showing three stages in the right-to-left swing of the abdomen of a swimming larva viewed from above. During the rapid flexural stage of the stroke (middle profile), the thoracic bristle tufts on the concave side of the body are bent forward in the direction of flow (dashed line). Open-headed arrows indicate the scissor-like motion of the anterior and posterior halves of the body. The filled circle at the junction of the thorax and abdomen indicates the position of the presumed centre of gravity of the larva.

numbers approach values of 1 and above, a bristled appendage functions more like a sieve and less like a paddle, but this transition is highly dependent on bristle spacing. Even at relatively high Reynolds numbers (1 and above), the leakiness index remains low if the bristle spacing is less than approximately 15 μm. The maximum velocity of the larval fan relative to the water during the rapid flexural stage of the stroke (Fig. 11C) is approximately $0.2\,m\,s^{-1}$. With a bristle diameter of 5 μm, the estimated local Reynolds number is approximately 1. Since the bristle spacing half-way along the fan is approximately 7 μm, the fan would be expected to behave as a continuous surface.

The thoracic bristle tufts present a more complex architecture than a simple array of bristles and cannot, therefore, be compared directly with the model of Cheer and Koehl (Cheer and Koehl, 1987). Although the bristle spacing is relatively large, the feather-like structure of the bristles, subdividing the inter-bristle space into pores of approximately 5 μm in width, suggests that, as in the abdominal fan, the bristle array is effectively non-porous. This would allow the thoracic tufts to function as paddles helping to establish a vortex at the anterior end of the body during rapid body flexion (Fig. 13C). Bristles of similar length to those of the thoracic tufts adorn the abdominal segments, but they are few in number and lack microtrichia. The morphological evidence therefore supports the idea that the thoracic tufts are specialised for a hydrodynamic role.

I am grateful to the Rutherford Appleton Laboratory, Oxford, for the loan of equipment from the EPSRC Engineering Instruments Pool. I should also like to thank Dee Hughes and Adrian Newman for help in graphics and artwork and Dawn Pammenter for typing the manuscript. An anonymous referee provided valuable comments on the analysis of circulation.

References

Blickhan, R., Krick, C., Zehren, D. and Nachtigall, W. (1992). Generation of a vortex chain in the wake of a subundulatory swimmer. *Naturwissenschaften* **79**, 220–221.

Brackenbury, J. H. (1999). Regulation of swimming in the *Culex pipiens* (Diptera, Culicidae) pupa: kinematics and locomotory trajectories. *J. Exp. Biol.* **202**, 2521–2529.

Cheer, A. Y. L. and Koehl, M. A. R. (1987). Paddles and rakes: fluid flow through bristled appendages of small organisms. *J. Theor. Biol.* **129**, 17–39.

Drucker, E. G. and Lauder, G. V. (1999). Locomotor force on a swimming fish: three-dimensional vortex wake dynamics quantified using digital particle image velocimetry. *J. Exp. Biol.* **202**, 2393–2412.

Gray, J. and Lissman, H. W. (1964). The locomotion of nematodes. *J. Exp. Biol.* **41**, 135–154.

Grodnitsky, D. L. (1999). *Form and Function in Insect Wings*. Baltimore, London: The Johns Hopkins University Press.

Kristan, W. B., McGirr, S. J. and Simpson, G. V. (1982). Behavioral and mechanosensory neurone responses to skin stimulation in leeches. *J. Exp. Biol.* **96**, 193–160.

Lighthill, M. J. (1969). Hydromechanics of aquatic animal locomotion. *Annu. Rev. Fluid Mech.* **1**, 413–446.

Lighthill, M. J. (1970). Aquatic propulsion of high hydrodynamic efficiency. *J. Fluid Mech.* **44**, 265–301.

Liu, H., Wassersug, R. J. and Kawachi, K. (1997). The three dimensional hydrodynamics of tadpole locomotion. *J. Exp. Biol.* **200**, 2807–2819.

McCutchen, C. W. (1977). Froude propulsive efficiency of a small fish, measured by wake visualisation. In *Scale Effects in Animal Locomotion* (ed. T. J. Pedley), pp. 339–363. London, New York, San Francisco: Academic Press.

Muller, V. K., Van den Heuvel, B. L. F., Stamhuis, E. J. and Videler, J. J. (1997). Fish foot prints: morphometrics and energetics of the wake behind a continuously swimming mullet (*Chelon labrosus* Risso). *J. Exp. Biol.* **200**, 2893–2900.

Nachtigall, W. (1961). Zur Locomotionsmechanik schwimmender Dipterenlarven. I. Mitteilung: Schwimmen ohne Ruderorgane: Ceratopogoniden und Chironomiden. *Z. Vergl. Physiol.* **44**, 509–522.

Nachtigall, W. (1962). Zur Locomotionsmechanik Dipterenpuppen. *Z. Vergl. Physiol.* **45**, 463–474.

Nachtigall, W. (1963). Zur Locomotionsmechanik schwimmender Dipterenlarven. Mitteilung: Schwimmen mit Ruderorganen: Culicinene und Corethrinen. *Z. Vergl. Physiol.* **46**, 449–466.

Rayner, J. M. V., Jones, E. and Thomas, A. (1986). Vortex flow visualizations reveal change in upstroke function with flight speed in bats. *Nature* **321**, 162–164.

Spedding, G. R. (1986). The wake of a jackdaw (*Corvus monedula)* in slow flight. *J. Exp. Biol.* **125**, 287–307.

Spedding, G. R. (1987). The wake of a kestrel (*Falco tinnunculus*) in flapping flight. *J. Exp. Biol.* **127**, 59–78.

Spedding, G. R., Rayner, J. M. V. and Pennycuick, C. J. (1984). Momentum and energy in the wake of a pigeon (*Columba livia*) in slow fight. *J. Exp. Biol.* **111**, 81–102.

Van den Berg, C. and Ellington, C. P. (1997). The vortex wake of a ‘hovering model hawk moth. *Phil. Trans R. Soc. Lond. B* **352**, 317–328.

Videler, J. B. (1993). *Fish Swimming*. London: Chapman & Hall. 260pp.

Wolfgang, M. J., Anderson, J. M., Grosenbaugh, M. A., Yue, D. K. P. and Triantophyllou, M. S. (1999). Near-body flow dynamics in swimming fish. *J. Exp. Biol.* **202**, 2302–2327.

Wu, T. Y. (1977). Introduction to the scaling of aquatic animal locomotion. In *Scale Effects in Animal Location* (ed. T. J. Pedley), pp. 203–232. London, New York, San Francisco: Academic Press.